0888-8809/07/$15.00/0
Printed in U.S.A.

Molecular Endocrinology 21(10):2579–2595

doi: 10.1210/me.2007-0245

Modulation of Human CYP19A1 Activity by Mutant NADPH P450 Oxidoreductase

Amit V. Pandey,* Petra Kempná,* Gaby Hofer, Primus E. Mullis, and Christa E. Flück

Pediatric Endocrinology, Diabetology & Metabolism, and Department of Clinical Research, University of Bern, CH-3010 Bern, Switzerland

Mutations in NADPH P450 oxidoreductase (POR) cause a broad spectrum of human disease with abnormalities in steroidogenesis. We have studied the impact of P450 reductase mutations on the activity of CYP19A1. POR supported CYP19A1 activity with a calculated K_m of 126 nM for androstenedione and a V_{max} of 1.7 pmol/min. Mutations R457H and V492E located in the FAD domain of POR that disrupt electron transfer caused a complete loss of CYP19A1 activity. The A287P mutation of POR decreased the activities of CYP17A1 by 60–80% but had normal CYP19A1 activity. Molecular modeling and protein docking studies suggested that A287P is involved in the interaction of POR:CYP17A1 but not in the POR:CYP19A1 interaction. Mutations C569Y and V608F in the NADPH binding domain of POR had 49 and 28% of activity of CYP19A1 compared with normal reductase and were more sensitive to the amount of NADPH available for supporting CYP19A1 activity. Substitution of NADH for NADPH had a higher impact on C569Y and V608F mutants of POR. Similar effects were obtained at low/high (5.5/8.5) pH, but using octanol to limit the flux of electrons from POR to CYP19A1 inhibited activity supported by all variants. High molar ratios of KCl also reduced the CYP19A1 supporting activities of C569Y and V608F mutants of POR to a greater extent compared to normal POR and A287P mutant. Because POR supports many P450s involved in steroidogenesis, bone formation, and drug metabolism, variations in the effects of POR mutations on specific enzyme activities may explain the broad clinical spectrum of POR deficiency. (*Molecular Endocrinology* 21: 2579–2595, 2007)

NADPH P450 OXIDOREDUCTASE (POR) (EC 1.6.2.4) transfers electrons from nicotinamide adenine dinucleotide phosphate (NADPH) to all microsomal type II P450 enzymes. The 32-kb gene (GI 94721356, NM_000941.2) for POR is located on chromosome 7q11.2 (1), has one untranslated exon (exon 1U) and 15 coding exons (2), and encodes a 82-kDa membrane-bound protein with 680 amino acids (NP_000932.3) (3). POR was initially identified by Horecker (4, 5) in 1950 as a cytochrome c reductase. Later studies by Williams and Kamin (6) and Phillips and Langdon (7) demonstrated this flavoprotein to be present in the endoplasmic reticulum (microsomes); subsequent studies in the 1960s and 1970s linked POR to the microsomal electron transport chains cytochromes P450 and b_5 involved in drug and steroid hydroxylations (8). The definitive evidence for the requirement of POR in cytochrome P450-mediated reactions came from the work of Lu *et al*. (8) who dissected the P450 containing mixed function oxidase system into three constituent components, POR, cytochrome P450, and lipids. The structure of POR is well understood from the x-ray crystal structures of the soluble, N-terminally deleted (N-63) form of rat POR (9) and FMN binding domain of human POR (10). This structure shows that POR has two distinct domains, one containing the NADPH-binding site and the FAD-binding domain, and the other containing the FMN domain that interacts with the redox-partner binding site of the P450s. The FMN domain is located at the N terminus of the POR and is structurally similar to flavodoxins, whereas the FAD/NADPH domain is located at the C terminus and is similar to ferredoxin reductases. The N terminus of POR has a 25- to 30-amino-acid-long hydrophobic sequence that serves as an anchor to position the POR toward the cytosolic side of the endoplasmic reticulum and is important for interaction with cytochrome P450s. Deletion of this N terminal leads to loss of P450 reductase activity of POR (8, 11). The domains that bind the FAD and FMN moieties are separated by a flexible hinge region. The electron transfer in POR from NADPH occurs in the form of two equivalents of hydride ion transfer to FAD moiety (12, 13). There are 50 genes encoding microsomal P450s that have been identified from the human genome (14); of these, 20 are involved in the biosynthesis of cholesterol, steroid hormones, fatty acids, and eicosanoids; 15 are involved in hepatic drug me-

First Published Online June 26, 2007

* A.V.P. and P.K. contributed equally to this work.

Abbreviations: ABS, Antley Bixler syndrome; 3D, three-dimensional; K_m, Michaelis constant; MD, molecular dynamics; NADPH, nicotinamide adenine dinucleotide phosphate; POR, NADPH P450 oxidoreductase; V_{max}, maximum velocity; WT, wild type.

***Molecular Endocrinology* is published monthly by The Endocrine Society (http://www.endo-society.org), the foremost professional society serving the endocrine community.**

tabolism; and 15 are "orphans" with unknown catalytic activities (14, 15). Because all these enzymes depend on POR for electron supply, disruption of POR may affect all microsomal P450 enzyme activities with disastrous consequences. Consistent with this, the POR knockout mouse results in early embryonic lethality (16, 17). Recently, we have identified more than 20 different POR mutations in over 34 patients with apparent combined 17α-hydroxylase, 21-hydroxylase deficiency (OMIM 201750) and a broad spectrum of clinical characteristics ranging from severe neonatal skeletal malformations with genital ambiguity [known as Antley Bixler syndrome (ABS); OMIM 207410], to phenotypically minor polycystic ovary syndrome-like features (18–24). Subsequent to our initial report, Arlt *et al.* (25) identified another POR missense mutation, Y181D (reported as Y178D), and also reported three of the POR mutations (A287P, R457H, and C569Y) that we had originally described. In a larger follow-up study, we have examined the POR genes in 19 additional patients (19). Fifteen of 19 patients having abnormal genitalia and disordered steroidogenesis were homozygous or apparent compound heterozygous for POR mutations that destroyed or dramatically inhibited POR activity. Most missense mutations were found once, but A287P was found on 10 alleles, and R457H was found on seven alleles. Thus, these two missense mutations accounted for 17 of 34 (50%) of the identified POR missense mutations. The A287P mutation was found only in samples from subjects described as "white," "Caucasian," or "European." This same mutation was also found on two (of eight) alleles in our initial report (18) in individuals of European heritage. Thus, A287P is a frequent mutation causing POR deficiency in this group. The R457H mutation was found in four of eight alleles from Japanese patients. This same mutation was also found on one (of two) Japanese alleles in our initial report (18) and on two of four alleles (26) and 10 of 16 alleles (27) in two subsequent reports of Japanese patients. Thus, R457H is strongly associated with alleles of Japanese heritage (28). In the recent reports from other laboratories, several new POR variants have been described (28–30). A G5G variant of POR has recently been reported to be associated with increased breast cancer risk in African-American women (31).

POR-dependent, steroidogenic type II P450 enzymes include CYP17A1 (17α-hydroxylase/17,20 lyase), CYP21B1 (21-hydroxylase), and CYP19A1 (aromatase). CYP17A1 is essential for the synthesis of glucocorticoids through its 17α-hydroxylase activity and for the synthesis of all sex steroids through its 17α-hydroxylase and 17,20 lyase activities (32). CYP21B1 catalyzes 21-hydroxylation of mineralocorticoids and glucocorticoids, and CYP19A1 converts androgens to estrogens, specifically androstenedione to estrone, testosterone to estradiol, and 16α-hydroxytestosterone to estriol (33). CYP19A1 is encoded by CYP19 that belongs to the family 19 of the P450 proteins (14, 34). It is expressed in many different tissues including the ovaries, testes, placenta, adipose tissue, and bone osteoblasts (33). CYP19A1 is localized in the endoplasmatic reticulum of the cell and catalyzes a unique three-step reaction (Fig. 1). The first two oxidative steps are cytochrome P450 hydroxylations, and the third step is a ferric peroxide removal of the aldehyde moiety, followed by aromatization of the steroid A-ring. Each step of the reaction requires a pair of electrons that are supplied from NADPH through POR.

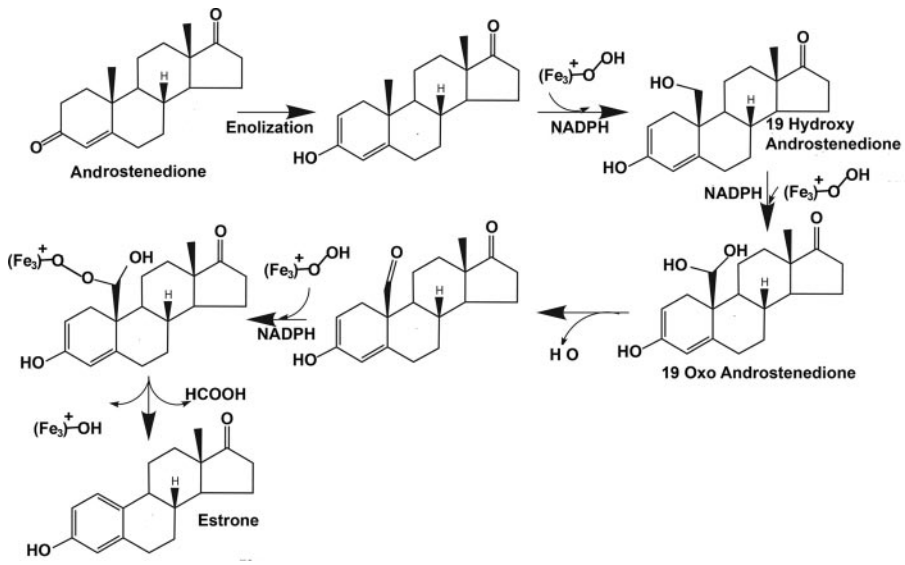

Fig. 1. Schematic Diagram of Reactions Catalyzed by CYP19A1

The reaction catalyzed by aromatase involves conversion of the ring A of the steroid structure to an aromatic ring with the loss of the angular C-19 methyl group and the cis-eliminaion of the 1β and 2β hydrogens to yield estrogen and formic acid. Note: this three-step reaction needs three pairs of electrons provided by NADPH.

Functional testing of our initial POR mutations using the classical cytochrome c assay and CYP17A1 (17α-hydroxylase/17,20 lyase) activity assays revealed partially conflicting results indicating that different POR variants may impact supported enzymatic reactions to variable degrees (18, 19). There were three distinct features of the POR mutations that we have originally described in our first report and that we are now addressing in more detail. First, mutations in the FAD region that destroy the binding of FAD to POR resulted in total loss of activity in both CYP17A1 and cytochrome c-based assays and therefore, should be almost inactive with all substrates. Second, the mutation A287P, found mostly in European patients, is in a location in POR that is not directly involved in the function of the electron transport and has close to wild-type (WT) activity with cytochrome c assay but lower activity with CYP17A1 assays. So it is possible that A287 is involved in the interaction of POR to P450s and other electron acceptors, and depending on its role in interacting with a particular acceptor protein, it may have variable effects on the activity of particular proteins. Third, the mutations in the NADPH binding domain of POR showed a higher Michaelis constant (K_m) for NADPH in cytochrome c-based assay. However, CYP17A1 was assayed with fixed NADPH concentration of 1 mM, which is more than 5000 times higher than the apparent K_m of POR for NADPH in cytochrome c-based assays. Therefore it is conceivable that the variations in the NADPH concentration might play a role in activity of these mutants and that a P450 with a faster reaction or requiring higher amounts of NADPH may be affected to a greater extent by mutations in the NADPH binding domain of POR than most other POR-dependent proteins.

To test these three hypotheses concerning different POR mutants, we coexpressed WT human CYP19A1, which requires three pairs of electrons for its activity, together with WT or mutant POR in yeast to obtain recombinant proteins for performing enzyme kinetic studies. We then compared kinetic data for POR-supported CYP19A1 activity with CYP17A1 activities. We used variations in assay conditions that limit the electron flux between POR and CYP19A1 to assess the impact on different mutations of POR. Finally, we built three-dimensional (3D) protein models for CYP19A1, CYP17A1, and POR and performed computational protein docking studies to understand better the structure-function relationship of various POR mutants and their impact on P450 activities.

RESULTS AND DISCUSSION

CYP19A1 Activity Supported by WT or Mutant POR

To assess the effect of WT or mutant POR on CYP19A1 activity we coexpressed both proteins in yeast W(B) (35), prepared microsomes, and tested them for the ability to convert [^{3}H]androstenedione to estrone, thereby releasing tritiated water (36). We decided to use microsomal preparations containing P450 and POR in our reactions instead of purified POR-P450-reconstituted systems for several different reasons. First, in our humanized yeast system we were able to express full-length aromatase in a similar fashion as we have expressed P450c17 for enzyme kinetic analysis in previous studies (18, 37). Western blot analysis confirmed that engineered yeast microsomes contained similar amounts of both WT or mutant POR as well as WT aromatase. Second, various methods available to reconstitute POR with P450 proteins give variable results in different laboratories. The reconstituted systems using phospholipids give best activity at a POR:P450 ratio of 1:5, and activity drops once this ratio is exceeded (38). This ratio and resulting activities vary depending on the type of P450 used and may not provide a standard value to compare P450 activities. Another concern was that these methods were optimized with normal POR in mind and changes brought by purification processes that may affect different POR variants to different degrees may add another level of complication that needs to be resolved separately for each POR variant before purified preparations of variant POR could routinely be used in all P450 reactions.

Kinetic studies of CYP19A1 reaction converting androstenedione to estrone revealed a K_m of 126.3 nM and a maximum velocity (V_{max}) of 1.70 pmol/min·mg protein (Table 1). Previously published enzyme kinetic studies found K_m values for the conversion of androstenedione by human CYP19A1 ranging from 100 to 260 nM when assaying N-terminally modified recombinant human CYP19A1 expressed either in insect cells (39) or in *E. coli* (40). Thus our novel, yeast-based functional assay seemed a reasonable system for studying the influence of POR variants on CYP19A1 activity.

In our previous report of the first POR mutations, we had identified the POR missense mutations A287P, R457H, and V492E in patients with the severe ABS skel-

Table 1. Calculated Kinetic Constants for CYP19A1 Activity with POR Variants Using Androstenedione as Substrate

	Apparent K_m (nM)	V_{max} (pmol/min)	V_{max}/K_m
WT	126.3 ± 10.4	1.70 ± 0.28	13.45
A287P	74.6 ± 15.2	1.04 ± 0.23	13.96
R457H	60.2 ± 18.4	0.01 ± 0.002	0.17
V492E	n.d.	n.d.	n.d.
C569Y	171.2 ± 31.8	1.18 ± 0.17	6.88
V608F	78.1 ± 22.9	0.25 ± 0.08	3.24

Values are mean ± SD of triplicate data sets. Experimental conditions are as described in *Materials and Methods*. n.d., Conversion activity too small (<1%); therefore, kinetic constants were not determined.

etal malformation phenotype, genital ambiguities, and disordered steroidogenesis, whereas the POR mutations C569Y and V608F were found in a young woman with normal breast development who was infertile and had polycystic ovaries and mild arterial hypertension (18, 41). Testing the effect of those POR variants on CYP17A1 activities *in vitro*, we found a loss of both 17α-hydroxylase and 17,20 lyase activities of CYP17A1 for the POR mutations R457H and V492E, a severe decrease of both activities for A287P, but only a mild inhibition for C569Y and V608F. Thus, our *in vitro* assay for CYP17A1:POR reflected the clinical findings in those patients. For POR-supported CYP19A1 activity, we found that compared with WT POR, A287P and C569Y inhibited CYP19A1 activity moderately and V608F significantly; however, when CYP19A1 activity was tested with POR R457H and V492E, enzymatic activity was completely lost (Fig. 2A). Calculations for enzyme kinetic constants revealed values that are summarized in Table 1. The catalytic efficiency (V_{max}/K_m) of CYP19A1 supported by POR variant A287P was similar to WT POR, but catalytic efficiency of POR mutants C569Y and V608F was significantly lower and was almost unmeasurable for POR R457H and V492E (Table 1).

POR Mutants A287P, C569Y, and V608F Have Variable Effects on CYP19A1 and CYP17A1 Activities

POR is the obligate electron transfer partner for both steroidogenic enzymes CYP19A1 and CYP17A1. We have tested the influence of different POR variants on the activities of CYP17A1 (18, 19) by identical methods as we have now used to test their influence on CYP19A1 activity; therefore, we were able to compare the impact of specific POR mutants on both enzymes directly (Fig. 2B). For POR mutants R457H and V492E, which are located in a highly conserved FAD binding domain (Fig. 2, C and D), enzymatic activities of both the CYP17A1 and CYP19A1 were lost. In contrast, POR mutants A287P, C569Y, and V608F were found to affect the activities of CYP17A1 and CYP19A1 to different degrees (Fig. 2B). Mutation A287P exerted no inhibitory effect on CYP19A1 activity compared with WT POR but was found to decrease 17α-hydroxylase to 20% and 17,20 lyase to 10% of WT activity (18). Conversely, we found a more prominent inhibitory effect of POR mutants C569Y and V608F, which are both located in the NADPH binding domain (Fig. 2C), on CYP19A1 activity than on CYP17A1 activities (25–50% *vs.* 50–80%; Fig. 2B and Ref. 18). Thus, different POR variants may affect diverse P450 activities to different degrees, explaining the broad spectrum of clinical phenotypes.

POR Mutants R457H and V492E Are Located in the FAD Domain and Disrupt Electron Transfer to Any Interacting P450

POR mutations R457H and V492E, which were found to cause a loss of both CYP19A1 and CYP17A1 activities, are located in the FAD domain of the POR protein (Fig. 2D). The FAD binding domain (residues 450–492) is highly conserved, and the sequence RYYSI (457–461) is invariant among human, rat, and yeast POR. The x-ray crystal structure of rat POR suggests that R457 forms a hydrogen bond with the pyrophosphate group of FAD, and Y459 contacts the FAD isoalloxazine ring and hydrogen bonds with the ribityl 3′-hydroxyl group (9, 42). Mutation R457H abolished all measurable activity of CYP19A1 similar to CYP17A1 activities (Fig. 2B). Similar results were obtained when these mutations were studied in rat POR (42–44). Residues 488–494, which lie in helix N, form hydrogen bonds with the FAD pyrophosphate. The mutation V492E, which is predicted to disrupt hydrogen bonds with FAD, has no activity. Thus, we conclude that mutations in the FAD domain of POR that directly interfere with the binding of FAD may affect all depending P450 enzyme activities severely because mutations in this location will hamper the ability of POR to transfer electrons to the FMN group of POR that ultimately provides electrons to P450s. Diminished FAD binding to R457H and V492E mutants of POR has recently been demonstrated (45).

3D Models of CYP19A1 and CYP17A1

Our CYP17A1 and CYP19A1 models were based on structures of mammalian P450 that have become available in the past couple of years. Both models showed that typical P450 fold around I helix and heme binding sites are in agreement with the structures of other mammalian P450 structures. CYP19A1 model had a fold typical of mammalian P450 structures with well-defined C, D, E, G, H, I, J, K, and L helices forming the structure. The helix F was in two distinct parts even after extensive MD refinement and could be a feature for providing access to different substrates of CYP19A1 because it was found to be quite flexible (Fig. 3). Models had energy values and structure parameters close to experimental structures (Table 2). Structural models of CYP19A1 based on bacterial P450 structures have been described previously (46, 47). In the later effort a consensus core structure based on structures of soluble bacterial P450s was employed to build the initial model, and less conserved residues and loops were added separately (47). Although the major features of the P450 structure like heme binding region and I-helix that constitutes the width of the molecule were found to be similar in the bacterial P450-based model, the substrate access channel and N-terminal helices were found to be slightly different from our model. A kink in the I-helix of CYP19A1 that is caused by sequence A-A-P was predicted in the earlier model and was also present in our model structure. More recently, structural models of CYP19A1 have been built based on mammalian P450 structures (48, 49). A model of CYP19A1 published recently that is based on the structure of rabbit P450 2C5 has similar features as our model (49). In the bacterial structure-based model, H105 was proposed

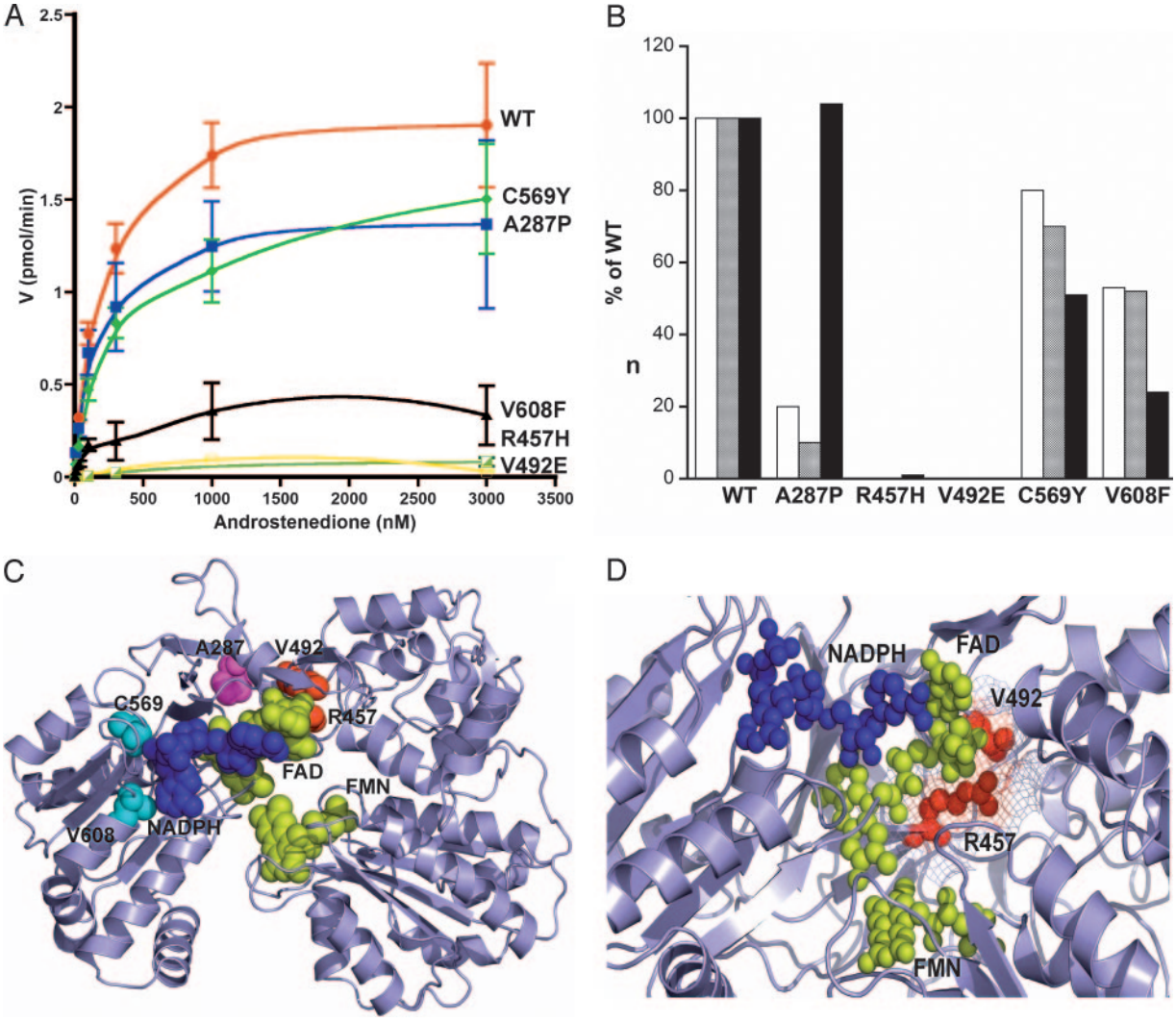

Fig. 2. Localization of POR Mutations and Their Effect on CYP19A1 Activity

A, Human CYP19A1 activity supported by WT or mutant POR. Yeast strain W(B) lacking endogenous CPR was transfected with both human WT *CYP19* and WT or mutant POR expression vectors. Microsomes containing CYP19A1 and POR proteins were prepared and their activity to convert [^{3}H] labeled androstenedione to estrone was tested by the tritiated water release assay (36). Kinetic data are presented in a *fitted plot*. The calculated K_m and V_{max} values are summarized in Table 1. ●, *Red line*, WT; ■, *blue line*, A287P; *light green line*, R457H; □, *yellow line*, V492E; ♦, *green line*, C569Y; ▲, *black line*, V608F. B, Catalytic efficiency of CYP19A1 activity supported by WT or mutant POR compared with both 17α-hydroxylase and 17,20 lyase activities of CYP17A1. Catalytic efficiency was calculated as V_{max}/K_m (Table 1) and plotted as percentage of WT. To compare the effect of POR variants on different P450s, we have included the equivalent values calculated for the 17α-hydroxylase and 17,20 lyase activities of CYP17A1, which we have tested in a similar fashion previously (18). *White columns*, 17α-Hydroxylase activity; *gray*, 17,20 lyase activity; *black*, CYP19A1 activity. C, POR mutations in the model structure of human P450 oxidoreductase. A 3D model of human POR showing the position of amino acids A287, R457, V492, C569, and V608. The POR model is based on the crystal structure of rat POR (PDB no. 1AMO) that shares 96% amino acid similarity with human POR. Protein is shown as a ribbon model and colored *light blue*. Arginine 457 and valine 492 are shown in *red*, alanine 287 is shown in *magenta*, and cysteine 569 and valine 608 are in *cyan*. FAD and FMN are shown in *yellow*, and NADPH is shown in *blue*. D, Localization and impact of POR mutations R457H and V492E. A closeup view of the FAD binding domain of POR showing the positions of amino acids R457 and V492. POR is shown as a *blue ribbon* model, FAD and FMN groups are shown in *yellow spheres*, and NADPH is shown as a *blue sphere* model. Amnio acids R457 and V492 are shown in *red sphere* models. The van der Walls surface of amino acids R457 and V492 is shown as a mesh model to emphasize the location and interaction with FAD group. POR mutations R457H and V492E are located in the FAD domain of the POR protein, and R457 forms a hydrogen bond with the pyrophosphate group of FAD. Mutation R457H results in complete loss of POR enzymatic activity. Amino acids V492 in POR is involved in stabilization of FAD group by forming hydrogen bonds. A change to glutamic acid results in disruption of FAD binding that leads to total loss of enzymatic activity of POR. The mutations in the FAD domain of POR, which destabilize the binding of FAD, may severely damage the electron transfer process because in the absence of FAD group in the POR the electrons from NADPH could not be transferred to the FMN group of POR or to its partner proteins. Protein model was edited with the programs Pymol and DeepView and rendered as a ray-traced image with POVRAY.

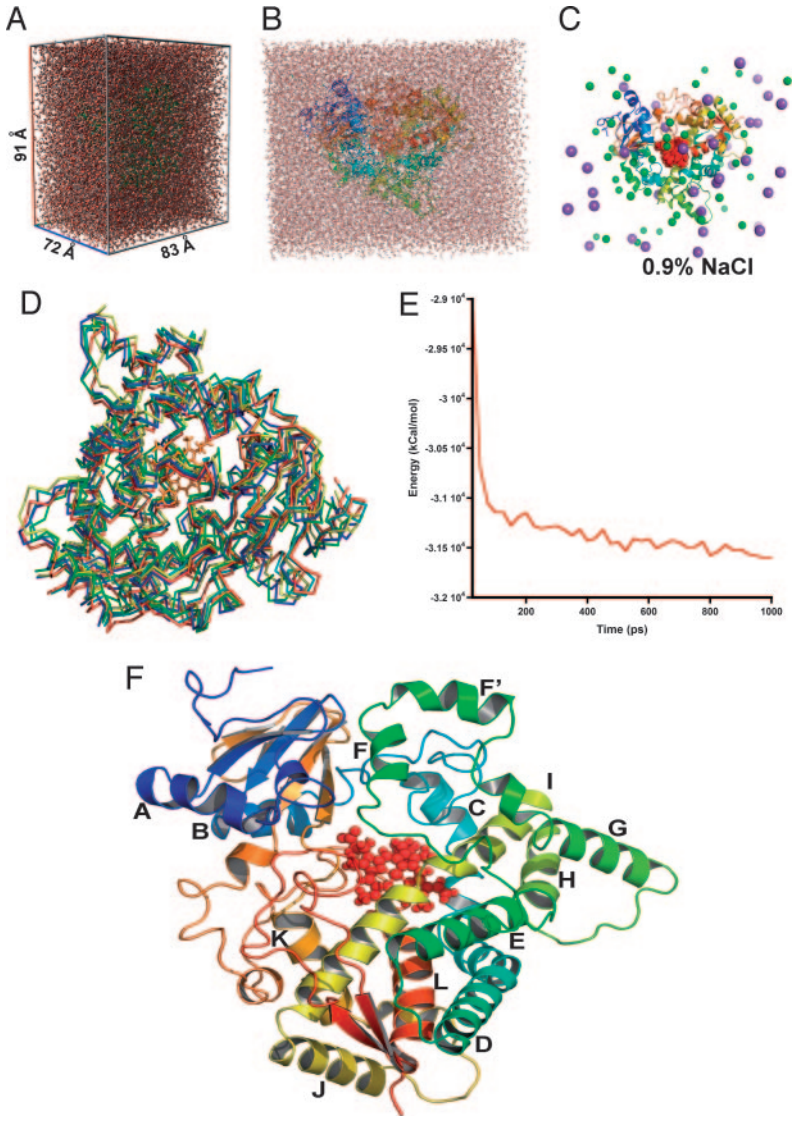

Fig. 3. Construction of the 3D Protein Model of Human CYP19A1

Model of CYP19A1 was based on crystal structure of human P450 3A4. Several rounds of refinements and energy minimization steps were performed to achieve the final model of CYP19A1. Model building is described under *3D protein models*. A, Refinement of CYP19A1 model by MD simulations. For MD refinement a simulation cell was constructed around the model with a cubic area extending 7.9 Å around each side of the model protein structure. Simulation cell was filled with water (B) and cell neutralization was performed to bring the pH to 7.0 by placing sodium and chloride ions as necessary (C). Sodium and chloride ions used to neutralize the cell are depicted as *purple* and *green spheres*. An initial 5-psec energy minimization step was carried out to distribute the solvents around the molecule, and final MD simulation was carried out using AMBER99 force-field for 500 psec at 298 K. After simulation, MD trajectories were analyzed, and snapshots obtained at different time intervals were evaluated for model quality parameters (D). After final model was selected among various candidates, a 1000-psec MD simulation was run for refinement. E, A plot of MD simulation trajectory is shown with total energy plotted against simulation time. F, Final model of CYP19A1. Model shows typical fold of P450 proteins with a dominant I helix across the molecule.

to be pointing toward solvent and had similar position in our (CYP3A4-based) model and the CYP2C5-based model. However, K150 present on helix C that was proposed to interact with heme propionate was far away from heme in mammalian P450-based models, and this position is taken by R145 in our model and R130 in the CYP3A4 structure. One of the heme propionates in our CYP19A1 model is stabilized by K119 and R375, whereas R435 and R145 stabilize the other propionate; these positions are R105, R375, R130, and R440 in CYP3A4 structure. A cysteine at position 437 that provides the fifth ligand for heme iron in CYP19A1 is conserved across all P450s and was modeled similarly in the bacterial as well as mammalian P450-based models. A 3D model for CYP17A1 based on a bacterial P450 structure has been described previously (50). In our CYP17A1 model, R96, H373, R125, and R440 provide propionate ligands,

Table 2. Parameters for Evaluation of Model Quality for CYP19A1 and CYP17A1 Model Structures

Evaluation Parameter	CYP3A4 (PDB id 1tqn)	CYP19A1 Model	CYP2B4 (PDB id 1suo)	CYP17A1 Model
RMS deviation		1.4		1.7
RMSZ bond length	0.469	0.560	0.689	0.963
RMSZ bond angle	0.738	0.716	0.836	1.027
RMSZ improper dihedrals	0.506	0.627	0.424	0.784
Inside/outside distribution	1.073	1.152	1.006	1.115
Ramachandran plot score	−2.643	−2.625	0.4	−0.871
Total energy (kJ/mol)	−13,347	−19,255	−19,027	−18,573

Parameters for the crystal structures are taken from PDBreport (78) database from WHATIF server. RMSD calculations were performed with DALI (83).

whereas C442 is linked to heme iron. In the CYP17A1 model from Auchus and Miller (50), neither R96 nor R125 is pointing toward heme propionate, and only R441 was identified as the correct ligand for heme propionate. A mutation in H373 has been reported to have complete loss of CYP17A1 activities (51), but H373 does not bind heme propionate in the model of Auchus and Miller (50) but was a ligand of heme in our model. In the CYP21B1 model described by us previously, R91, R124, H365, and R426 were found to associate with heme propionates (52). These positively charged amino acids are conserved across all mammalian P450s (H369 and H368 in CYP2C5 and CYP2B4 structures), and use of a bacterial P450 template for model seems to have caused this discrepancy in the model of Auchus and Miller. Other major structural features like the presence of a T group at the catalytic center in I helix, an R group in K helix, and W in C helix were in the same positions in both our model and the model of Auchus and Miller. Cytochrome P450s have quite variable N-terminal regions as compared with C-terminal region containing the meander region/heme binding site and I, J, K, and L helices that are well conserved. Earlier modeling efforts that were based on bacterial P450 structures had to rely on extensive refinement of the variable region, which often had to be modeled separately and led to incorrect assignment for some critical residues. Another advantage of using P450 3A4 structure as template is that testosterone, a substrate of CYP19A1, is also metabolized by CYP3A4 and, therefore, may have the region around substrate access and binding that is likely to be closer to the CYP19A1 structure.

POR Mutant A287P Interferes with the Interaction of POR:CYP17A1 But Not of POR:CYP19A1

To investigate why POR mutant A287P is able to support CYP19A1 as well as WT POR but exerts an inhibitory effect on CYP17A1 activities, we performed detailed protein structure–function analysis. In the 3D model of human POR as well as in crystal structure of rat POR, the amino acid alanine 287 is located in the back side of the POR molecule, below the FAD binding region, and does not seem to play any direct role in the activity of POR (Fig. 2C). But because A287 may play a role in the interaction with P450s, we analyzed the interaction of POR with CYP17A1 and CYP19A1 by molecular docking studies. Models of CYP19A1 and CYP17A1 were built based on 3D crystal structures of CYP3A4 and CYP2B4, respectively, and docking of POR with either CYP17A1 or CYP19A1 was performed. Model evaluation parameters are given in Table 2 and Fig. 3. Interaction of CYP17A1 with POR involves location of CYP17A1 behind the FMN and FAD domains of POR so that C-terminal arginines of CYP17A1 are in close proximity to negatively charged amino acids in the FMN domain of POR (Fig. 4A). Amino acid alanine 287 is located at the start of a loop in POR that is interacting with the C-terminus loop of CYP17A1, and possibly the interaction of these loops plays a role in correct positioning of CYP17A1 with POR (Fig. 4B). A change from alanine to proline will break the loop in POR at the beginning, and as a consequence the interacting loop in CYP17A1 will no longer be in close proximity with POR. In Fig. 4C, a close-up of the interface of the POR:CYP17A1 interaction is shown where the loop involving A287 and the C-terminal loop on CYP17A1 are visible. In contrast, interaction of POR with CYP19A1 does not seem to involve amino acid A287 of POR because CYP19A1 interacts with POR mostly from the front side of the FMN domain and the space between FMN and NADPH domain (Fig. 4D). This rules out any damaging effect of the POR A287P mutant on the activity of CYP19A1.

POR Mutants C569Y and V608F, Located in the NADPH Binding Domain, Are More Susceptible to Cofactor Concentrations

The NADPH binding domain of POR is highly conserved, especially the sequence GTGVAP (residues 534–539), which contains the consensus GXG sequence typical of $NADP^+$-binding proteins (53, 54). However, the details of NADPH binding to POR are not clearly understood because the electron density of the nicotinamide ring is not well defined in the crystal structure of rat POR, and subsequently there is significant spatial disorder in this region of the structure.

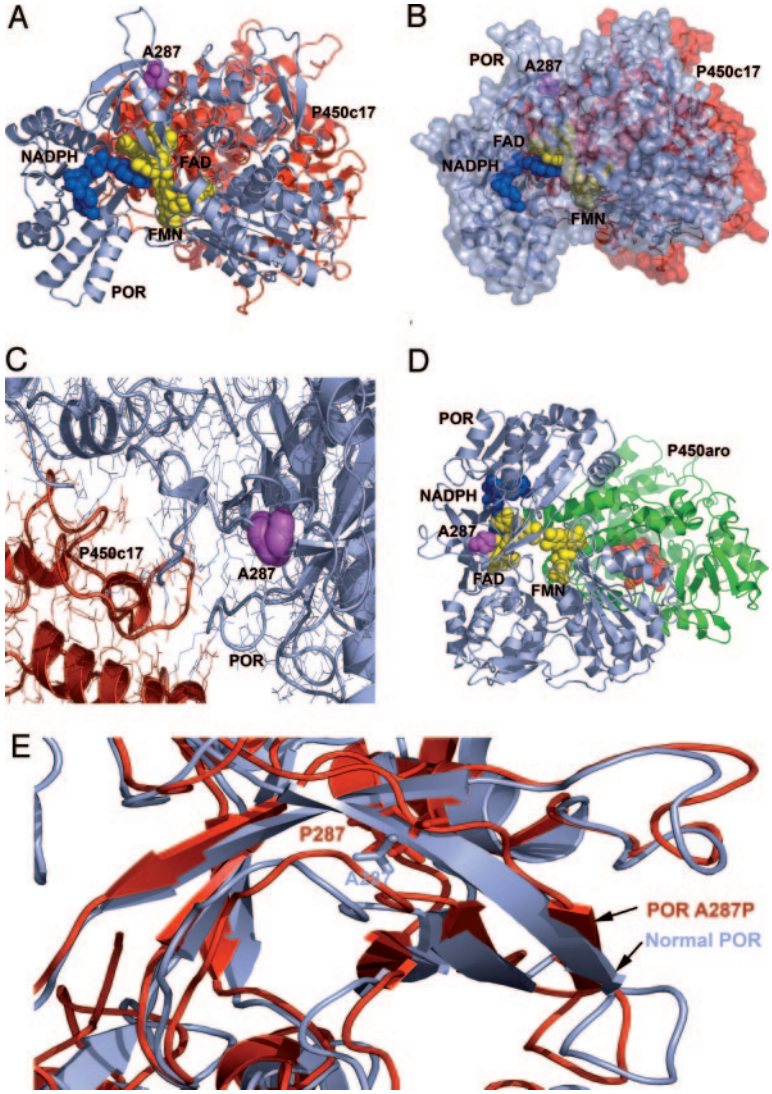

Fig. 4. Interaction of Amino Acid A287 of POR with CYP19A1 and CYP17A1

Models of CYP19A1 and CYP17A1 were based on 3D crystal structures of P450 3A4 and P450 2B4, respectively, and docking of POR with either CYP17A1 or CYP19A1 was performed using the programs Hex4.5 and Patchdock. A, Docking model of POR interacting with CYP17A1. Amino acid alanine 287 is located at the start of a loop in POR that is interacting with the C-terminal loop of CYP17A1, and change from alanine to proline will break the loop at the beginning so that the loop in CYP17A1 will no longer be in close proximity with POR. One of the docking solutions is shown here with POR in *blue ribbon* and CYP17A1 in *red ribbon*. B, The surface of CYP17A1 is shown with 60% transparency to emphasize the position of amino acid 287 (shown in *magenta*). In POR FAD and FMN groups are shown as *yellow spheres* and NADPH is shown as a *blue sphere* model. C, A close-up of the POR:CYP17A1 interaction interface is shown where the loop involving A287 and the loop on CYP17A1 interacting with POR are visible. D, Protein docking model of POR interacting with CYP19A1. CYP19A1 is shown as *green ribbon* and POR as *blue ribbon*. CYP19A1 does not seem to be in contact with the loop harboring POR A287. E, Superimposition of normal and A287P variant POR structure. The A287P mutation was performed *in silico* and MD simulation was performed to calculate the structural implications of this mutation. Normal POR is shown in *light blue* and altered (A287P) structure is shown in *red*. Changes to β-sheets and loops in the POR structure after A287P mutations are probably responsible for altered activity profile. Protein models were edited with Pymol and rendered as ray-traced images with POVRAY.

Several residues have been proposed to bind the NADPH in the POR that include Ser599, Arg600, and Lys605. These residues are believed to provide specificity for NADPH binding in POR as compared with NADH. Both cysteine 569 and valine 608 are located in the NADPH binding domain of POR (Fig. 5). In the 3D structure of rat POR as well as model of human POR, cysteine 569 interacts with NADPH with distances of 3.05 and 3.42 Å (for human POR). A change from cysteine to tyrosine will change the binding of NADPH and will result in reduction of efficiency for the mutated POR. Studies in which C569 of human POR was alkylated with iodoacetic acid eliminated activity, implicating a role for cysteine in binding of NADPH to

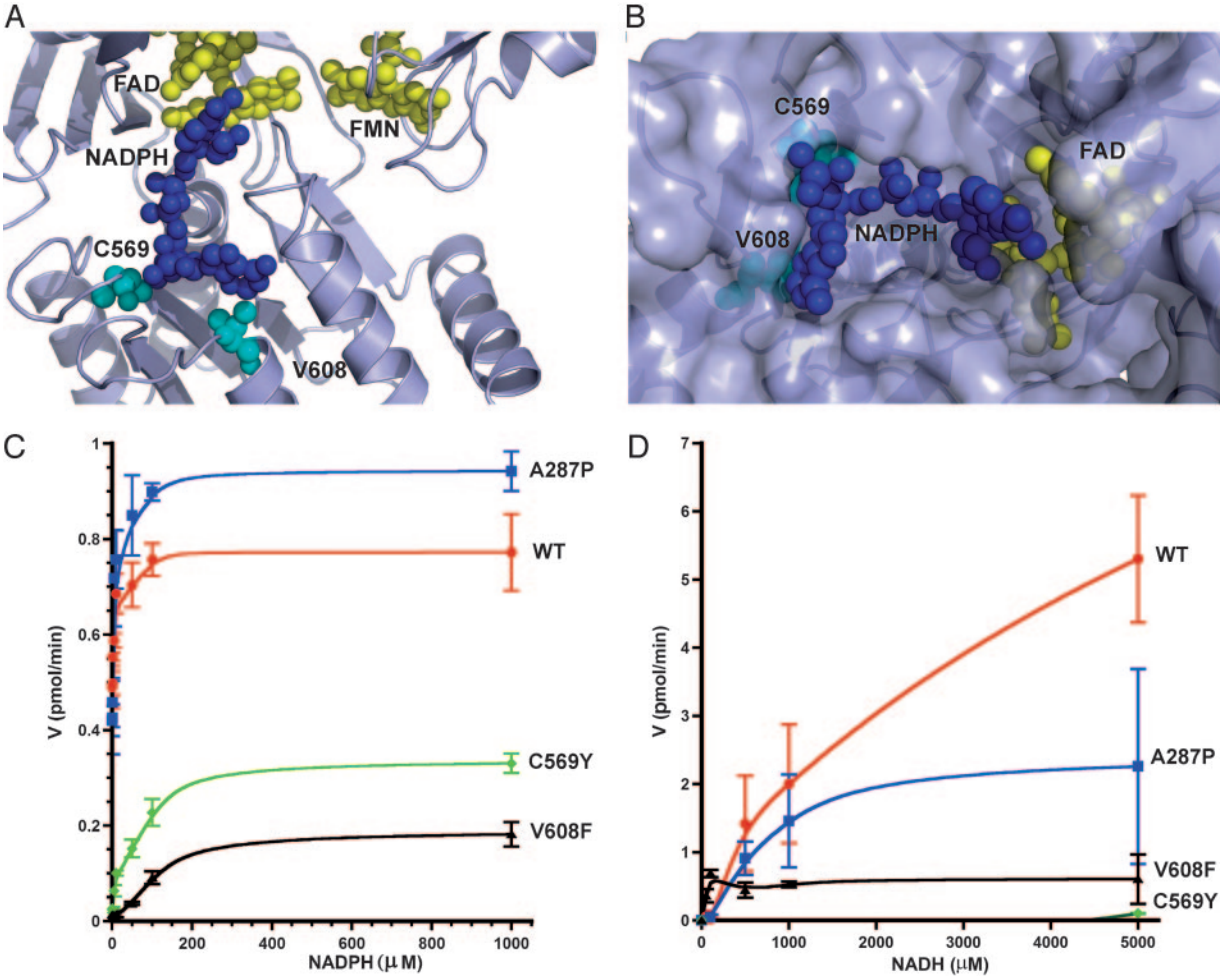

Fig. 5. Mutations in NADPH Binding Region and Effect of Cofactor Variation of POR Activities

Model of human POR showing the positions of mutations V608F and C569Y**.** A, POR is shown as a ribbon diagram colored in *light blue*, and cofactor NADPH is shown as a sphere model in *dark blue*. Valine 608 and cysteine 569 are shown as *cyan spheres*. Both valine 608 and cysteine 569 are in the NADPH binding domain of POR; in the 3D structure of rat POR as well as model of human POR, cysteine 569 interacts with NADPH with distances of 3.05 and 3.42 Å (for human POR). A change from cysteine to tyrosine will change the binding of NADPH and will result in reduction of efficiency for the mutated POR. Valine 608 is next to 604 tyrosine, which interacts with first orthophosphate group of NADPH with a distance of 2.96 Å. A change from valine to phenylalanine would interfere with the NADPH binding site. B, The NADPH binding cavity of POR is shown here as a transparent surface model with secondary structural elements of POR shown in ribbon model. NADPH is shown in *blue spheres*, and valine 608 and cysteine 569 are shown in *cyan spheres* inside the cavity. Both these amino acids are providing the anchoring points for the binding of NADPH to the cavity. A part of the FAD group is also visible as a *yellow sphere* model. The model was rendered with Pymol, and ray-traced image was generated with POVRAY. C, Effects of cofactor variations on activity of CYP19A1 supported by WT or variant POR. Effect of variable concentrations of NADPH on POR supported CYP19A1 activity. Microsomes containing WT POR or POR mutants A287P, C569Y, V608F, and WT CYP19A1 were incubated with a fixed amount of [^{3}H]-labeled substrate (100 nM androstenedione) but variable amounts of NADPH (0.05–1000 μM) as a cofactor providing electrons. CYP19A1 activity was quantitated indirectly by assessing the release of tritiated water during the reaction (36). ●, *Red line*, WT; ■, *blue line*, A287P; ♦, *green line*, C569Y; ▲, *black line*, V608F. D, Effect of substitution of NADH as cofactor on POR supported CYP19A1 activity. Microsomes containing WT POR or POR mutants A287P, C569Y, V608F, and WT CYP19A1 were incubated with a fixed amount of [^{3}H]-labeled substrate (100 nM androstenedione) but variable amounts of NADH (0.05–5000 μM) as an alternative cofactor for providing electrons. CYP19A1 activity was quantitated indirectly by assessing the release of tritiated water during the reaction (36). ●, *Red line*, WT; ■, *blue line*, A287P; ♦, *green line*, C569Y; ▲, *black line*, V608F.

human POR (3). But mutagenesis of the C569 to S in rat POR suggested that this residue was not essential, despite a 4.6-fold higher K_m value for NADPH (55), and alkylation of pig POR did not change activity (56). The mutation C569Y in human POR, which we previously described in a patient with disordered steroidogenesis but without ABS (18) also had a high K_m for NADPH in the cytochrome c assay, but retained 70% of 17,20 lyase activity and 80% of 17α-hydroxylase activity. The C569Y mutation was found as a compound het-

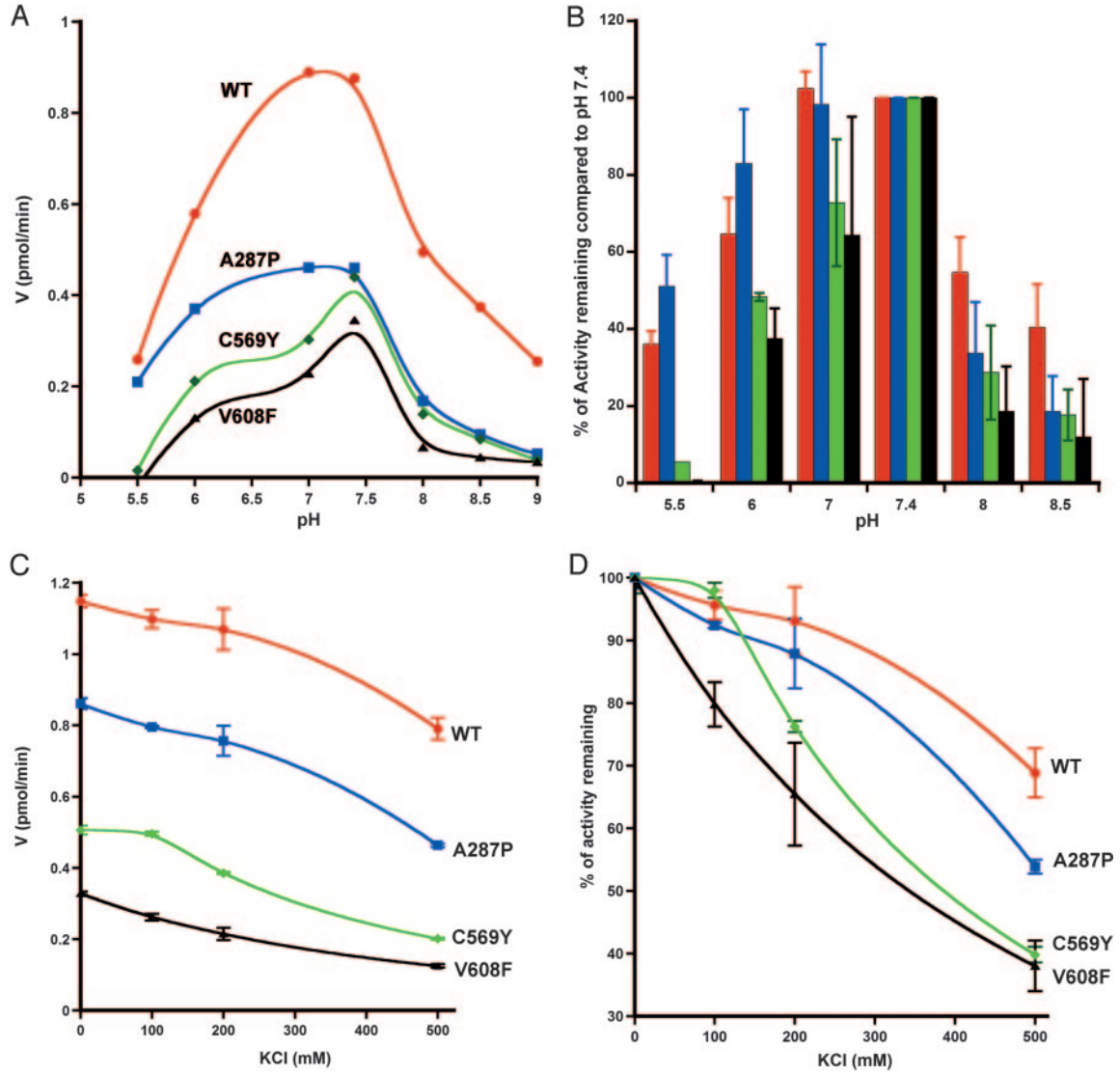

Fig. 6. Perturbation of Reaction Conditions and Altered POR Activities

Effect of pH on POR supported CYP19A1 activity. A, pH response curve of CYP19A1 activity supported by WT and mutant POR. Microsomes containing either WT POR or POR mutants A287P, C569Y, V608F, and WT CYP19A1 were incubated with a fixed amount of [^{3}H] labeled substrate (100 nM androstenedione) and NADPH (1 mM) as the cofactor providing electrons. Reactions were carried out at different pH values to assess the effect of pH on interaction of POR with CYP19A1. CYP19A1 activity was quantitated indirectly by assessing the release of tritiated water during the reaction (36). ●, *Red line*, WT; ■, *blue line*, A287P; ♦, *green line*, C569Y; ▲, *black line*, V608F. WT CYP19A1 follows a bell-shaped curve with change in pH that is typical of enzymatic reactions under variable pH conditions. An optimum pH of 7–7.4 is obtained for WT POR. CYP19A1 activity supported by mutant POR also had 7.4 as pH optima. B, Comparison of POR supported CYP19A1 activity as percentage of optimum value. Activity at pH 7.4 was optimal for all POR variants and was taken as 100% for calculation of activities at different pH values. Normal and A287P variants of POR were relatively stable at low pH values, whereas POR variant C569Y and V608F lost almost all activity at pH 5.5. At higher pH values, all CYP19A1 reactions with mutant POR lost almost 80% of their pH 7.4 activity, whereas activity with WT POR retained 40% of its optimal value. *Red bars*, WT; *blue*, A287P; *green*, C569Y; and *black*, V608F. C and D, Effect of KCl on interaction of normal and mutant POR with CYP19A1. Microsomes containing WT POR or POR mutants A287P, C569Y, V608F, and WT CYP19A1 were incubated with a fixed amount of [^{3}H]-labeled substrate (100 nM androstenedione) and NADPH (1 mM) as a cofactor providing electrons. Potassium chloride was included at a concentration of 0 to 500 mM to perturb the interaction of POR with CYP19A1. CYP19A1 activity was quantitated indirectly by assessing the release of tritiated water during the reaction (36). ●, *Red line*, WT; ■, *blue line*, A287P; ♦, *green line*, C569Y; ▲, *black line*, V608F. Small amount of KCl has no adverse effect on P450 activities and is often included in preparation of homogenates and microsomes during P450 assays. However, high concentrations of KCl can disturb the electrostatic interaction between POR and P450 and lead to reduction of activities. Up to 200 mM concentration of KCl had only a mild effect on POR-supported activity, but increasing the KCl concentration to 500 mM resulted in loss of activity for C569Y and V608F, and binding of NADPH to POR seems to be affected by higher KCl concentrations, because inclusion of octanol as described earlier did not result in any specific effect for these POR variants. POR variant A287P did not lose as much activity, suggesting that general disturbances in POR-P450 interaction are not the only effects of higher KCl concentration. C, Total activity plotted against increasing KCl concentration. D, Percentage of activity remaining compared with activity in the absence of KCl, plotted against increasing KCl concentration.

erozygote with V608F (18) which retained 52% of 17,20 lyase activity and 53% of 17α-hydroxylase activity. Valine 608 is next to tyrosine 607 and lysine 605 which have several contacts with NADPH, especially between OH group of tyrosine and first orthophosphate group of NADPH with a distance of 2.96 Å and second orthophosphate group of NADPH is at a distance of 2.49 Å from lysine 605. A change from valine to phenylalaline will disturb the NADPH binding site. However, an excess of NADPH may be able to overcome some of the binding defect because binding does not seem to be completely destroyed.

Conversion of androgens to estrogens by human CYP19A1 depends on the transfer of three pairs of electrons from NADPH through POR (Fig. 1). In contrast, CYP17A1 activities for the conversion of both steps, first pregnenolone to 17α-hydroxypregnenolone (by 17α-hydroxylase), and second to dehydroepiandrosterone (by 17,20 lyase) require only one pair of electrons per reaction (15). Therefore, we thought that the differential inhibition of POR mutants C569Y and V608F on CYP17A1 and CYP19A1 might be due to a difference in cofactor requirement. So we assayed CYP19A1 activity supported by constant amounts of WT, A287P, C569Y, and V608F POR protein but different concentrations of NADPH (Fig. 5C). WT and A287P POR needed approximately 5 nM NADPH for half maximal CYP19A1 activity (calculated EC_{50}). By contrast, C569Y and V608F required 76–108 nM NADPH. Consistent with that, mutations in the NADPH binding domain also show a higher K_m for NADPH in cytochrome c assays (18, 19). Thus, POR mutations in the NADPH binding domain seem to impair CYP19A1 activity more when cofactor availability is limited. In line with these *in vitro* findings, the single reported patient harboring two POR mutations in the NADPH binding domain manifested with a very mild, polycystic ovary syndrome-like phenotype consistent with only CYP19A1 deficiency (18).

POR Mutants C569Y and V608F Have Diminished Capacity for NADH as Electron Donor Compared with WT POR

A change from cysteine to tyrosine seems to have higher impact on binding of NADH and results in reduced binding efficiency for the POR mutation C569Y. The mutation C569Y, which has a higher K_m for NADPH in the cytochrome c assays, has almost no activity when NADH was substituted for NADPH as the electron donor (Fig. 5D). Valine 608 on the other hand is not directly involved in the binding of NADPH and has some activity with NADH as substrate, implying a less critical role for V608 than C569 in the cofactor binding. In general, both C569Y and V608F mutations that lie in the NADPH binding site of POR resulted in severely diminished activities when NADH is used as a substrate compared with NADPH. Normal and A287P mutant of POR also showed reduced activities with NADH as substrate, but the effects were much less compared with C569Y and V608F mutants of POR.

Effect of Changes in pH on Activity of CYP19A1 Supported by Normal and Mutant POR

We have used several different methods to vary the interaction between POR and CYP19A1 to assess the impact of variable electron flux on changes in the activity of CYP19A1 supported by different POR mutants. One such method is to change the pH of the reaction in the assay of CYP19A1 activity (57). The pH profile of CYP19A1 activity supported by normal POR follows a bell-shaped curve with optimum pH between 7.0 and 7.4, and mutant enzymes also show optimum pH around 7.4 (Fig. 6A). However, there are remarkable variations in the responses of different POR variants at pH values higher or lower than optimum pH. At pH 5.5, up to 35% of optimal CYP19A1 activity supported by normal POR (obtained at pH 7.4) is retained (Fig. 6B). However, CYP19A1 activity supported by C569Y mutant drops to less than 10% and mutant V608F has almost no activity at pH 5.5. At higher pH values, the effects are a little less remarkable but the same pattern is observed. At pH 8.5, normal POR retained more than 40% of its optimal activity, and activities of A287P, C569Y, and V608F mutants fell below 20% of their optimal values (Fig. 6B). Higher pH seems to destabilize A287P variant of POR to a greater extent than low pH conditions because at pH 5.5 and 6.0, the A287P mutant of POR retains greater than 50 and 80% activities, respectively.

Changes in Membrane Order by Addition of Octanol in CYP19A1 Reaction Reduce Activity But Are Not Specific for Any POR Mutant

Addition of n-alkanols has been used previously to alter the membrane order in CYP19A1 activity assays (57). We used variable concentrations of octanol in the reaction mixture during assay of CYP19A1 activity to change the membrane order of microsomes containing CYP19A1 and POR and perturb the interaction of POR with CYP19A1. We used 0 to 50 mM octanol in our reactions to alter the membrane conditions based on previous results and found that normal and A287P mutant of POR retained only 25% of their activity in the presence of 50 mM octanol (Table 3). Effects on C569Y and V608F mutants were also in the same range. This suggests that changes in general conditions that limit the POR interaction with P450 do not differentiate between the variant POR studied by us. However, any mutations on the surface of POR that might be involved in interaction with P450 might show a different response to changes in membrane order that affect the POR-P450 interaction.

Effect of KCl on CYP19A1 Activity Supported by Normal and Mutant POR

Generally KCl has only a mild effect on P450 activities, and only at KCl concentrations of 250 mM or higher is

Table 3. Effect of Increasing Octanol Concentration on the Activity of CYP19A1 Supported by WT or Variant POR

Octanol (mM)	POR WT	POR A287P	POR C569Y	POR V608F
0	0.775 ± 0.003	0.672 ± 0.013	0.36 ± 0.0123	0.224 ± 0.011
5	0.538 ± 0.093	0.473 ± 0.067	0.216 ± 0.016	0.139 ± 0.003
15	0.382 ± 0.072	0.488 ± 0.013	0.127 ± 0.008	0.079 ± 0.008
30	0.247 ± 0.021	0.205 ± 0.010	0.092 ± 0.002	0.068 ± 0.005
50	0.172 ± 0.009	0.237 ± 0.017	0.094±0.008	0.092 ± 0.003

Data are expressed as mean ± SD for CYP19A1 activity (pmol/min) in triplicate experiments. Reactions were carried out as described in *CYP19A1* activity assay. A fixed substrate concentration of 100 nM androstenedione and 1 mM NADPH was used.

a significant decrease in activity observed. We observed this pattern for the normal and A287P variant of POR (Fig. 6C). However, C569Y and V608F variants showed much reduced activities around 200 mM KCl and lost more than 60% of their activities at 500 mM KCl (Fig. 6D). In comparison, WT POR retained more than 80% activity, and the A287P mutant retained more than 60% of its activity, suggesting a milder effect by higher KCl concentrations. Some destabilization in the A287P mutant may be responsible for greater reduction in activity compared with normal POR. Increased loss of activities by C569Y and V608F mutants suggests alterations in NADPH binding under these conditions that have greater impact on POR with mutations in the NADPH binding site. Reduction in activity of P450 at high KCl concentrations is attributed to disruption of charged pair electrostatic interactions between POR and P450, but the higher impact on mutations C569Y and V608F is probably due to diminished binding of NADPH or slower release of NADP in the cofactor binding pocket of POR.

In summary, our detailed studies of POR-supported CYP17A1 and CYP19A1 activities suggest that different POR mutations can affect dependent P450s differently. Mutations in the FAD domain, which disrupt electron transfer, will affect all microsomal P450s. Mutations in the NADPH domain may affect P450s with high electron requirement more severely. Cofactor specificity of POR seems to be affected even more by mutations in the NADPH binding site. Normal POR has preference for NADPH over NADH by several orders of magnitude in the K_m values, which are in millimolar range for NADH but lie in nanomolar to submicromolar range for NADPH. Similar results were observed in this study for CYP19A1 reaction. However, C569Y mutation seems to lose almost all capacity to bind and use NADH as an alternate electron donor. Limiting the cofactor availability by other methods of perturbation like inclusion of alcohol or salt enabled us to differentiate the effects in general POR-P450 interactions compared with specific changes in cofactor utilization. POR mutations C569Y and V608F can interact with P450s like normal POR as evidenced by relatively minor changes in apparent K_m of P450 substrates for the P450s in both CYP17A1 and CYP19A1 reactions studied by us. Changing the POR-P450 interaction by membrane perturbation induced by octanol results in a general reduction of CYP19A1 activities. However, some changes by inclusion of octanol/KCl or change in pH could be due to altered protein conformation. Some indication of this is suggested from relatively higher loss of activity supported by A287P mutant of POR under low pH and high KCl concentrations. Further studies on folding and conformation of different POR mutants will shed more light on these differences.

Finally, some POR mutations may be located in the interaction face of some POR:P450 complexes, hampering the interaction between some partners but not affecting others. In reconstituted systems, P450 proteins form a complex with POR with an apparent K_m of around 0.2 μM. The P450:POR interaction is influenced by many factors including type of P450, availability of substrates, and ionic strength of the system (58). The interaction of POR with cytochrome P450 and other electron acceptor proteins is based primarily on electrostatic charge pairing, although there is evidence for an additional hydrophobic component. The surface of the electron-donating (FMN) domain of POR is characterized by acidic residues (9, 59, 60), whereas the redox-partner binding site of microsomal P450 enzymes is typically characterized by basic residues (61–63). Chemical cross-linking and modification studies have shown that POR contains multiple carboxylate groups, presumably contributed by the acidic amino acids aspartate and glutamate (59, 64). These charge groups pair with basic amino acids (lysines, arginines) on the various electron acceptor proteins (65–67). Thus electrostatic interactions that pair charges are obviously important in governing the association of POR with a P450 enzyme. Chemical modification of acidic residues in the FMN site of POR reduces the activity of P450 (59, 64, 68). Perturbation in the membrane and electrostatic environment of POR-P450 reactions by changes in pH/KCl and inclusion of n-alcohols will be able to differentiate these mutations.

In addition, cytochrome P450 forms a dipole across the molecule, with the positive charge at the proximal face of the protein where the heme makes its closest approach to the surface. This is thought to be the surface most suitable for electron transfer from POR. Although electrostatic forces may serve to connect and orient the partners, hydrophobic forces contributed by nonpolar amino acids (leucine, tryptophan, valine, *etc.*) may be responsible for bringing the two proteins close enough together for electron transfer (69). Other electron acceptor proteins, such as cyto-

chrome b_5, heme oxygenase, and squalene monooxygenase, probably interact by the same mechanism. POR interacts with and supports the enzymatic activities of all 50 human microsomal P450 enzymes. The activities assessed in different P450 studies are not only a function of the specific P450 enzyme used as the read-out of the POR activity, but also a function of the form of POR used. Both the full-length POR used in our first report and the N-27 human POR used in our bacterial expression system remain associated with membranes and are able to support the reduction of a cytochrome P450 (41). By contrast, when rat or human POR is rendered wholly soluble by deleting 57 N-terminal residues, it can still reduce cytochrome c but cannot reduce a P450 (8, 11). Because the interactions of POR with different P450 enzymes will vary with the geometry of the redox-partner binding site of the P450, no assay based on a single P450 enzyme will reliably forecast all the consequences of a specific POR mutant. Only the residues that severely affect the FAD or FMN binding may lose all enzymatic activity and could be tested by employing the cytochrome c-based assays along with a single P450-based assay (41). By contrast, those POR mutations that are involved in POR:P450 interactions may have to be tested with many different P450 assays to establish the exact nature of their impact on individual P450 reactions. Because all 50 microsomal P450 enzymes depend on POR for electron supply, we are putting forward the hypothesis that defects in POR may cause disorders in hepatic drug and xenobiotic metabolism as well as affect the functions of all steroid metabolizing microsomal P450 enzymes.

MATERIALS AND METHODS

Plasmid Constructs

Yeast expression vector pYeSF1-pgk was built by inserting the constitutively active *pgk* (phosphoglycerate kinase) promoter in the yeast vector pYeSF1 (37). In brief, *pgk* promoter was cleaved from yeast vector V10 using *Bgl*II and *Bam*HI restriction sites. The fragment was then cloned into *Bam*HI site of pYeSF1 resulting in pYeSF1-pgk vector containing an *ade*2 selection marker. CYP19A1 cDNA was amplified with Long Template Polymerase (Roche, Basel, Switzerland) using plasmid pcDNA3-ARO (70) as template and the following primers AroF: 5′TCCCCCGGGAGCC**ATG**GTTTTGGAAATGCTGAACCCGA; and AroR: 5′TCCCCCGGG**CTA**GTGTTCCAGACACCTGTCTGAGTTTC (restriction sites are *underlined*, start and stop codons are shown in *bold*). The PCR product was cloned into the pYeSF1-pgk vector through the *Sma*I restriction site. Correctness of the resulting construct pYeSF1-pgk-ARO was confirmed by direct sequencing (Microsynth, Basel, Switzerland). Construction of human WT and mutant POR cDNAs A287P, R457H, V492E, C569Y, and V608F into pYcDE2 has been described previously (18). Numbering of the amino acids of the POR protein is based on NCBI NP_000932.3 and corresponds to the full length, 680 amino acid human POR sequence.

Expression of Human CYP19A1 and POR

Yeast strain W(B) lacking the endogenous yeast CPR1 gene (35, 71, 72) was propagated and transiently cotransfected with pYcDE2 expressing full-length WT or mutant POR cDNAs and pYeSF1-pgk-ARO expressing human WT CYP19A1. Yeast microsomes were prepared as described (37), and microsomal proteins were quantitated colorimetrically (Protein Assay Dye Reagent, Bio-Rad, Hercules, CA). To control for equal expression, Western blot analyses of microsomal proteins were performed using a rabbit polyclonal antibody against human placental CYP19A1 kindly provided by Dr. Nobuhiro Harada (73), and a rabbit polyclonal antibody against POR commercially available from Stressgen Bioreagents (LuBioScience GmbH, Lucerne, Switzerland).

CYP19A1 Activity Assay

The ability of POR to support the activity of CYP19A1 was assayed with yeast microsomal proteins containing human CYP19A1 and WT or mutant human POR as electron donor. CYP19A1 activity was measured by the release of tritiated water from 1β-^{3}H substrates during aromatization as described by Lephart and Simpson (36). Briefly, reactions were performed in 15-ml Falcon tubes in a final volume of 200 μl at 37 C. Yeast microsomes (40 μg microsomal protein/reaction) were incubated with 0.01–3 μM cold androstenedione, and a constant amount of [1β-^{3}H(N)]-androstene-3,17-dione (40,000 cpm/reaction) in 50 mM K-phosphate buffer (pH 7.4). Reactions were initiated by adding 1 mM NADPH (unless indicated differently). Reactions were stopped by adding 1 ml of chloroform. The mixture was vortexed for 30 sec, then 1 ml of water was added, and the mix was centrifuged at 1000 rpm for 5 min. Aliquots of the water phase (0.5 ml) were taken and mixed with an equal volume of 5% charcoal/0.5% dextran. After 40 sec of extraction, samples were centrifuged at 12,000 rpm for 15 min, and 0.5-ml aliquots of supernatants were collected for counting of ^{3}H radioactivity. The measured cpm values were corrected for background radioactivity and multiplied by a factor of 4 because actual counted aliquots represented only one fourth of the total reaction volume. Once percentage conversion of androstenedione to estrone was assessed, further calculations were performed to describe the kinetic characteristics of WT CYP19A1 when supported by either WT or mutant POR. Nonlinear regression was used for this analysis. Curve fitting and calculation of V_{max} and apparent K_m values were performed using PRISM 3.02 (GraphPad Software Inc., San Diego, CA). Data represent the mean ± SD of two to four independent experiments, each performed in duplicate.

Buffers involving different pH values for measuring the effect of pH on CYP19A1 activities were prepared separately at twice the working concentration and substituted for normal buffer in the reactions involving measurements at alternate pH values. Experiments involving the presence of octanol were carried out by addition of octanol in the reaction mixture before addition of substrate and NADPH. Total alcohol volume did not exceed 5% of the reaction volume, and after an incubation of 5 min at room temperature the reaction was started by addition of substrate and NADPH. Similarly KCl was added from a stock solution of 5.0 M in the reactions involving measurement of CYP19A1 activity at different concentrations of KCl. In one set of experiments NADH was substituted for NADPH as the source of electrons.

3D Protein Models

3D structural models of CYP19A1, POR, and CYP17A1 were generated to study the potential impact of POR mutations on interaction with CYP19A1 and CYP17A1. A phi BLAST search of the protein structure database was performed against the CYP19A1 (NP_000094) and CYP17A1 (NP_000093) amino

acid sequences, which revealed the recently solved structure of human P450 3A4 (74) (PDB no. 1tqn) (NP_059488) as the closest match for CYP19A1, and rabbit P450 2B4 structure (PDB no. 1suo) (75) was identified as the template for modeling human CYP17A1. We first performed a multiple sequence alignment of CYP19A1 with the human P450 sequences from PDB database including steroidogenic CYP17A1 and CYP21B1 by CLUSTALW (http://www.ebi.ac.uk/clustalw) (76) to analyze the structural features of the CYP19A1 protein sequence. We then performed a structural alignment of P4503A4 and CYP19A1 and used that for model building with the program MODELLER 8 (77). For the CYP17A1 model, we have used our previously described alignment for P450 2B4 structure and CYP21B1 and CYP17A1 sequences (52). Basic protocols for model building for CYP19A1 and CYP17A1 models were as described previously (52). The model was subjected to energy minimization and then checked by the programs WHATCHECK (http://swift.cmbi.ru.nl/gv/whatcheck) (78), Verify3D (79) (http://nihserver.mbi.ucla.edu/Verify_3D), and PROCHECK (80) (http://biotech.embl-ebi.ac.uk:8400/) and by Ramachandran plot analysis (81, 82) for abnormalities in the structure. Calculations for RMSD values were performed with DALI (83). Several rounds of model building and optimizations were performed to finally obtain a model that was energetically stable and passed the tests for the quality of the structure. CYP17A1 model was also generated in similar fashion based on 3D structure of rabbit P4502B4. For human POR, we used our previously described 3D protein model, which is based on the structure of rat POR (9) (PDB id 1AMO) (NP_113764) that shares 96% sequence similarity with human POR (NP_000932). The WT protein model was used to create mutants of POR with the program DEEPVIEW (84). Altered structures were subjected to energy minimization using molecular dynamics (MD) simulation and checked by WHATIF (http://swift.cmbi.kun.nl/whatif/) (85) and WHATCHECK (78) to remove bumps in the sidechains with respect to neighboring amino acids that were caused by *in silico* mutations. Coordinates of computer models are available as PDB files upon request. Models were depicted with Pymol (www.pymol.org) and rendered as ray-traced images with POVRAY (www.povray.org).

MD Simulation for Model Refinement

The MD simulations were performed using YASARA dynamics (86). A simulation cell (91 $\times$ 72 $\times$ 83 Å) was constructed around the CYP19A1 homology model with a 7.9 Å cutoff for Lennard-Jones forces and the direct space portion of the electrostatic forces, which were calculated using the Particle Mesh Ewald method. The pKa values of the ionizable groups in the model were predicted and assigned the protonation states based on pH 7.0. The cell was filled with water, and the AMBER99 (87) electrostatic potential was evaluated at all water molecules; the one with the lowest or highest potential was turned into a sodium or chloride counter ion until the cell was neutral. A short steepest descent minimization of all atoms was done to remove severe bumps in the protein and to achieve convergence until the maximum atom speed dropped below 2200 m/sec. Then a start-up simulation was run for 5 psec, using a multiple time step of 1 fsec for intramolecular and 2 fsec for intermolecular forces, with all heavy protein atoms fixed, so that the solvent molecules could smoothly cover the protein surface. Simulated annealing minimizations were started at 298 K, and velocities were scaled down every 10 steps for a total time of 5 psec in 500 steps. We then ran MD simulations with AMBER99 force field at 298 K and 0.9% NaCl in the simulation cell for 1000 psec to refine the models. All MD computations were run locally on a Dell computer server containing 4 intel CPUs running under SUSE Linux 10.1/Windows server 2003. A local installation of WHAT IF program was used to check the quality of models in combination with Verify3D analysis to check for abnormalities. An analysis of MD trajectories showed a significant improvement, and final model snapshot has a free energy of -19255 kJ/mol for CYP19A1 model. The Cα-RMSD dropped from an initial value of 2.7 Å, which is typical for a decent homology model to 1.4 Å, which corresponds to a medium-resolution x-ray structure. Using the MD simulation, we could refine the homology model close to an experimental-like structure. Modeling of P450 proteins has recently been quite successful, and some of the models of P450 show very high similarity when compared with the actual structures which have recently become available (88). An increase in the number of mammalian P450 structures that have become available recently combined with powerful computational hardware and software for modeling side-chains and loops in the variable regions of homology models could be attributed to this achievement.

Analysis of the Interaction of POR with CYP19A1 and CYP17A1 by 3D Docking

We used the programs Patchdock (89) and Hex 4.5 (90) for analysis of the interaction of WT and A287P mutant of POR with CYP19A1 and CYP17A1. We performed the 3D protein-protein interaction analysis of the interaction of POR with either CYP19A1 or CYP17A1 to understand the role of alanine 287 in P450:POR interactions and whether a change to proline would affect such interactions. Electrostatic interactions are known to be involved between positively charged groups on P450s and negatively charged acidic residues on POR and were taken into consideration while calculating the dockings. In the first step, a molecular shape representation was performed by computing the molecular surface of the molecule. Next, a segmentation algorithm was applied for detection of geometric patches, which were filtered, and then a geometric hashing and pose-clustering matching was performed to match the patches on two structures. Concave patches were matched with convex and flat patches with any type of patches. The complexes obtained were then examined, and all complexes with unacceptable penetrations of the atoms of the receptor to the atoms of the ligand were discarded. Finally, the remaining candidates were ranked according to a geometric shape complementarity score. In total, 50,000 calculations were performed per pair, and solutions were filtered for energetically stable conformations. The top 20 solutions from each round of calculations were manually checked for interaction sites and orientation of the molecules. Structures were edited with the program Pymol and depicted and ray-traced images were generated by POVRAY.

Acknowledgments

We thank Prof. Walter L. Miller, University of California San Francisco (San Francisco, CA), and Dr. Nobuhiro Harada, Fujita Health University (Toyoake, Aichi, Japan) for support.

Received May 10, 2007. Accepted June 21, 2007.

Address all correspondence and requests for reprints to: Christa E. Flück, M.D., Pediatric Endocrinology and Diabetology, University of Bern, Freiburgstrasse 15, G3 812, CH-3010 Bern, Switzerland. E-mail: christa.flueck@insel.ch.

Address requests for materials and structure model files to: Amit V. Pandey, Ph.D., Department of Clinical Research, University of Bern, Tiefenaustrasse 120, CH-3004 Bern, Switzerland. E-mail: amit@pandeylab.org.

This work was supported by Swiss National Science Foundation Grants 3232B0103178/179 (to C.E.F.) and 3100A0-113719 (to A.V.P.).

The nucleotide sequence of the human NADPH P450 oxidoreductase gene is available in the NCBI nucleotide data-

base under NCBI accession no. NM_000941. The amino acid sequence of human POR can be accessed through NCBI Protein Database under NCBI accession no. NP_000932. The atomic coordinates for the crystal structure of rat POR are available in the Research Collaboratory for Structural Bioinformatics Protein Databank PDB no. 1AMO. The atomic coordinates for the crystal structure of FMN binding domain of human POR are available in the Research Collaboratory for Structural Bioinformatics Protein Databank PDB no. 1B1C. Online Mendelian Inheritance in Man, OMIM no. 124015, 201750. Enzyme collection number, EC 1.6.2.4.

Disclosure Statement: A.V.P., P.K., G.H., P.E.M., and C.E.F. have nothing to declare.

REFERENCES

1. Shephard EA, Phillips IR, Santisteban I, West LF, Palmer CN, Ashworth A, Povey S 1989 Isolation of a human cytochrome P-450 reductase cDNA clone and localization of the corresponding gene to chromosome 7q11.2. Ann Hum Genet 53:291–301
2. Scott RR, Gomes LG, Huang N, Van Vliet G, Miller WL 2007 Apparent manifesting heterozygosity in p450 oxidoreductase deficiency and its effect on coexisting 21-hydroxylase deficiency. J Clin Endocrinol Metab 92: 2318–2322
3. Haniu M, McManus ME, Birkett DJ, Lee TD, Shively JE 1989 Structural and functional analysis of NADPH-cytochrome P-450 reductase from human liver: complete sequence of human enzyme and NADPH-binding sites. Biochemistry 28:8639–8645
4. Horecker BL, Heppel LA 1949 The reduction of cytochrome c by xanthine oxidase. J Biol Chem 178:683–690
5. Horecker BL 1950 Triphosphate nucleotide-cytochrome c reductase in liver. J Biol Chem 183:593–605
6. Williams Jr CH, Kamin H 1962 Microsomal triphosphopyridine nucleotide-cytochrome c reductase of liver. J Biol Chem 237:587–595
7. Phillips AH, Langdon RG 1962 Hepatic triphosphopyridine nucleotide-cytochrome c reductase: isolation, characterization, and kinetic studies. J Biol Chem 237: 2652–2660
8. Lu AY, Junk KW, Coon MJ 1969 Resolution of the cytochrome P-450-containing ω-hydroxylation system of liver microsomes into three components. J Biol Chem 244: 3714–3721
9. Wang M, Roberts DL, Paschke R, Shea TM, Masters BSS, Kim JJ 1997 Three-dimensional structure of NADPH-cytochrome P450 reductase: prototype for FMN- and FAD-containing enzymes. Proc Natl Acad Sci USA 94:8411–8416
10. Zhao Q, Modi S, Smith G, Paine M, McDonagh PD, Wolf CR, Tew D, Lian LY, Roberts GC, Driessen HP 1999 Crystal structure of the FMN-binding domain of human cytochrome P450 reductase at 1.93 A resolution. Protein Sci 8:298–306
11. Roman LJ, McLain J, Masters BSS 2003 Chimeric enzymes of cytochrome P450 oxidoreductase and neuronal nitric-oxide synthase reductase domain reveal structural and functional differences. J Biol Chem 278: 25700–25707
12. Munro AW, Noble MA, Robledo L, Daff SN, Chapman SK 2001 Determination of the redox properties of human NADPH-cytochrome P450 reductase. Biochemistry 40: 1956–1963
13. Hubbard PA, Shen AL, Paschke R, Kasper CB, Kim JJ 2001 NADPH-cytochrome P450 oxidoreductase. Structural basis for hydride and electron transfer. J Biol Chem 276:29163–29170
14. Nelson DR, Zeldin DC, Hoffman SM, Maltais LJ, Wain HM, Nebert DW 2004 Comparison of cytochrome P450 (CYP) genes from the mouse and human genomes, including nomenclature recommendations for genes, pseudogenes and alternative-splice variants. Pharmacogenetics 14:1–18
15. Miller WL 2005 Minireview: regulation of steroidogenesis by electron transfer. Endocrinology 146:2544–2550
16. Shen AL, O'Leary KA, Kasper CB 2002 Association of multiple developmental defects and embryonic lethality with loss of microsomal NADPH-cytochrome P450 oxidoreductase. J Biol Chem 277:6536–6541
17. Otto DM, Henderson CJ, Carrie D, Davey M, Gundersen TE, Blomhoff R, Adams RH, Tickle C, Wolf CR 2003 Identification of novel roles of the cytochrome P450 system in early embryogenesis: effects on vasculogenesis and retinoic acid homeostasis. Mol Cell Biol 23: 6103–6116
18. Flück CE, Tajima T, Pandey AV, Arlt W, Okuhara K, Verge CF, Jabs EW, Mendonca BB, Fujieda K, Miller WL 2004 Mutant P450 oxidoreductase causes disordered steroidogenesis with and without Antley-Bixler syndrome. Nat Genet 36:228–230
19. Huang N, Pandey AV, Agrawal V, Reardon W, Lapunzina PD, Mowat D, Jabs EW, Van Vliet G, Sack J, Flück CE, Miller WL 2005 Diversity and function of mutations in p450 oxidoreductase in patients with Antley-Bixler syndrome and disordered steroidogenesis. Am J Hum Genet 76:729–749
20. Pandey AV, Flück CE, Huang N, Tajima T, Fujieda K, Miller WL 2004 P450 oxidoreductase deficiency: a new disorder of steroidogenesis affecting all microsomal P450 enzymes. Endocr Res 30:881–888
21. Pandey AV 2006 Biochemical analysis of mutations in P450 oxidoreductase. Biochem Soc Trans 34: 1186–1191
22. Miller WL 2004 P450 oxidoreductase deficiency: a new disorder of steroidogenesis with multiple clinical manifestations. Trends Endocrinol Metab 15:311–315
23. Miller WL, Huang N, Flück CE, Pandey AV 2004 P450 oxidoreductase deficiency. Lancet 364:1663
24. Miller WL, Huang N, Pandey AV, Flück CE, Agrawal V 2005 P450 oxidoreductase deficiency: a new disorder of steroidogenesis. Ann NY Acad Sci 1061:100–108
25. Arlt W, Walker EA, Draper N, Ivison HE, Ride JP, Hammer F, Chalder SM, Borucka-Mankiewicz M, Hauffa BP, Malunowicz EM, Stewart PM, Shackleton CH 2004 Congenital adrenal hyperplasia caused by mutant P450 oxidoreductase and human androgen synthesis: analytical study. Lancet 363:2128–2135
26. Adachi M, Tachibana K, Asakura Y, Yamamoto T, Hanaki K, Oka A 2004 Compound heterozygous mutations of cytochrome P450 oxidoreductase gene (POR) in two patients with Antley-Bixler syndrome. Am J Med Genet 128A:333–339
27. Fukami M, Horikawa R, Nagai T, Tanaka T, Naiki Y, Sato N, Okuyama T, Nakai H, Soneda S, Tachibana K, Matsuo N, Sato S, Homma K, Nishimura G, Hasegawa T, Ogata T 2005 Cytochrome P450 oxidoreductase gene mutations and Antley-Bixler syndrome with abnormal genitalia and/or impaired steroidogenesis: molecular and clinical studies in 10 patients. J Clin Endocrinol Metab 90: 414–426
28. Adachi M, Asakura Y, Matsuo M, Yamamoto T, Hanaki K, Arlt W 2006 POR R457H is a global founder mutation causing Antley-Bixler syndrome with autosomal recessive trait. Am J Med Genet A 140:633–635
29. Homma K, Hasegawa T, Nagai T, Adachi M, Horikawa R, Fujiwara I, Tajima T, Takeda R, Fukami M, Ogata T 2006 Urine steroid hormone profile analysis in cytochrome P450 oxidoreductase deficiency: implication for the backdoor pathway to dihydrotestosterone. J Clin Endocrinol Metab 91:2643–2649
30. Fukami M, Hasegawa T, Horikawa R, Ohashi T, Nishimura G, Homma K, Ogata T 2006 Cytochrome P450

oxidoreductase deficiency in three patients initially regarded as having 21-hydroxylase deficiency and/or aromatase deficiency: diagnostic value of urine steroid hormone analysis. Pediatr Res 59:276–280
31. Haiman CA, Setiawan VW, Xia LY, Le Marchand L, Ingles SA, Ursin G, Press MF, Bernstein L, John EM, Henderson BE 2007 A variant in the cytochrome p450 oxidoreductase gene is associated with breast cancer risk in African Americans. Cancer Res 67:3565–3568
32. Miller WL 1988 Molecular biology of steroid hormone synthesis. Endocr Rev 9:295–318
33. Simpson ER 2004 Aromatase: biologic relevance of tissue-specific expression. Semin Reprod Med 22:11–23
34. Nebert DW, Nelson DR, Feyereisen R 1989 Evolution of the cytochrome P450 genes. Xenobiotica 19:1149–1160
35. Pompon D, Perret A, Bellamine A, Laine R, Gautier JC, Urban P 1995 Genetically engineered yeast cells and their applications. Toxicol Lett 82–83:815–822
36. Lephart ED, Simpson ER 1991 Assay of aromatase activity. In: Waterman MR, Johnson EF, eds. Methods in enzymology. San Diego: Academic Press; 477–483
37. Auchus RJ, Lee TC, Miller WL 1998 Cytochrome b5 augments the 17,20-lyase activity of human P450c17 without direct electron transfer. J Biol Chem 273: 3158–3165
38. Reed JR, Kelley RW, Backes WL 2006 An evaluation of methods for the reconstitution of cytochromes P450 and NADPH P450 reductase into lipid vesicles. Drug Metab Dispos 34:660–666
39. Amarneh B, Simpson ER 1995 Expression of a recombinant derivative of human aromatase P450 in insect cells utilizing the baculovirus vector system. Mol Cell Endocrinol 109:R1–R5
40. Kagawa N, Hori H, Waterman MR, Yoshioka S 2004 Characterization of stable human aromatase expressed in *E. coli*. Steroids 69:235–243
41. Flück CE, Nicolo C, Pandey AV 2007 Clinical, structural and functional implications of mutations and polymorphisms in human NADPH P450 oxidoreductase. Fundam Clin Pharmacol 21:399–410
42. Shen AL, Kasper CB 2000 Differential contributions of NADPH-cytochrome P450 oxidoreductase FAD binding site residues to flavin binding and catalysis. J Biol Chem 275:41087–41091
43. Shen AL, Kasper CB 1996 Role of Ser457 of NADPH-cytochrome P450 oxidoreductase in catalysis and control of FAD oxidation-reduction potential. Biochemistry 35:9451–9459
44. Shen AL, Sem DS, Kasper CB 1999 Mechanistic studies on the reductive half-reaction of NADPH-cytochrome P450 oxidoreductase. J Biol Chem 274:5391–5398
45. Marohnic CC, Panda SP, Martasek P, Masters BS 2006 Diminished FAD binding in the Y459H and V492E Antley-Bixler syndrome mutants of human cytochrome P450 reductase. J Biol Chem 281:35975–35982
46. Graham-Lorence S, Khalil MW, Lorence MC, Mendelson CR, Simpson ER 1991 Structure-function relationships of human aromatase cytochrome P-450 using molecular modeling and site-directed mutagenesis. J Biol Chem 266:11939–11946
47. Graham-Lorence S, Amarneh B, White RE, Peterson JA, Simpson ER 1995 A three-dimensional model of aromatase cytochrome P450. Protein Sci 4:1065–1080
48. Loge C, Le Borgne M, Marchand P, Robert JM, Le Baut G, Palzer M, Hartmann RW 2005 Three-dimensional model of cytochrome P450 human aromatase. J Enzyme Inhib Med Chem 20:581–585
49. Favia AD, Cavalli A, Masetti M, Carotti A, Recanatini M 2006 Three-dimensional model of the human aromatase enzyme and density functional parameterization of the iron-containing protoporphyrin IX for a molecular dynamics study of heme-cysteinato cytochromes. Proteins 62: 1074–1087
50. Auchus RJ, Miller WL 1999 Molecular modeling of human P450c17 (17α-hydroxylase/17,20-lyase): insights into reaction mechanisms and effects of mutations. Mol Endocrinol 13:1169–1182
51. Monno S, Ogawa H, Date T, Fujioka M, Miller WL, Kobayashi M 1993 Mutation of histidine 373 to leucine in cytochrome P450c17 causes 17 α-hydroxylase deficiency. J Biol Chem 268:25811–25817
52. Janner M, Pandey AV, Mullis PE, Fluck CE 2006 Clinical and biochemical description of a novel CYP21A2 gene mutation 962_963insA using a new 3D model for the P450c21 protein. Eur J Endocrinol 155:143–151
53. Hanukoglu I, Gutfinger T 1989 cDNA sequence of adrenodoxin reductase. Identification of NADP-binding sites in oxidoreductases. Eur J Biochem 180:479–484
54. Scrutton NS, Berry A, Perham RN 1990 Redesign of the coenzyme specificity of a dehydrogenase by protein engineering. Nature 343:38–43
55. Shen AL, Christensen MJ, Kasper CB 1991 NADPH-cytochrome P-450 oxidoreductase. The role of cysteine 566 in catalysis and cofactor binding. J Biol Chem 266: 19976–19980
56. Haniu M, Iyanagi T, Legesse K, Shively JE 1984 Structural analysis of NADPH-cytochrome P-450 reductase from porcine hepatic microsomes. Sequences of proteolytic fragments, cysteine-containing peptides, and a NADPH-protected cysteine peptide. J Biol Chem 259: 13703–13711
57. Grogan J, Shou M, Zhou D, Chen S, Korzekwa KR 1993 Use of aromatase (CYP19) metabolite ratios to characterize electron transfer from NADPH-cytochrome P450 reductase. Biochemistry 32:12007–12012
58. Backes WL, Kelley RW 2003 Organization of multiple cytochrome P450s with NADPH-cytochrome P450 reductase in membranes. Pharmacol Ther 98:221–233
59. Shen AL, Kasper CB 1995 Role of acidic residues in the interaction of NADPH-cytochrome P450 oxidoreductase with cytochrome P450 and cytochrome c. J Biol Chem 270:27475–27480
60. Estabrook RW, Shet MS, Fisher CW, Jenkins CM, Waterman MR 1996 The interaction of NADPH-P450 reductase with P450: an electrochemical study of the role of the flavin mononucleotide-binding domain. Arch Biochem Biophys 333:308–315
61. Hasemann CA, Kurumbail RG, Boddupalli SS, Peterson JA, Deisenhofer J 1995 Structure and function of cytochromes P450: a comparative analysis of three crystal structures. Structure 3:41–62
62. Fisher CW, Shet MS, Estabrook RW 1996 Construction of plasmids and expression in *Escherichia coli* of enzymatically active fusion proteins containing the heme-domain of a P450 linked to NADPH-P450 reductase. Methods Enzymol 272:15–25
63. Davydov DR, Kariakin AA, Petushkova NA, Peterson JA 2000 Association of cytochromes P450 with their reductases: opposite sign of the electrostatic interactions in P450BM-3 as compared with the microsomal 2B4 system. Biochemistry 39:6489–6497
64. Nadler SG, Strobel HW 1991 Identification and characterization of an NADPH-cytochrome P450 reductase derived peptide involved in binding to cytochrome P450. Arch Biochem Biophys 290:277–284
65. Shen S, Strobel HW 1993 Role of lysine and arginine residues of cytochrome P450 in the interaction between cytochrome P4502B1 and NADPH-cytochrome P450 reductase. Arch Biochem Biophys 304:257–265
66. Shen S, Strobel HW 1992 The role of cytochrome P450 lysine residues in the interaction between cytochrome P450IA1 and NADPH-cytochrome P450 reductase. Arch Biochem Biophys 294:83–90
67. Shimizu T, Tateishi T, Hatano M, Fujii-Kuriyama Y 1991 Probing the role of lysines and arginines in the catalytic function of cytochrome P450d by site-directed mutagen-

esis. Interaction with NADPH-cytochrome P450 reductase. J Biol Chem 266:3372–3375
68. Nadler SG, Strobel HW 1988 Role of electrostatic interactions in the reaction of NADPH-cytochrome P-450 reductase with cytochromes P-450. Arch Biochem Biophys 261:418–429
69. Strobel HW, Nadler SG, Nelson DR 1989 Cytochrome P-450: cytochrome P-450 reductase interactions. Drug Metab Rev 20:519–533
70. Maffei L, Murata Y, Rochira V, Tubert G, Aranda C, Vazquez M, Clyne CD, Davis S, Simpson ER, Carani C 2004 Dysmetabolic syndrome in a man with a novel mutation of the aromatase gene: effects of testosterone, alendronate, and estradiol treatment. J Clin Endocrinol Metab 89:61–70
71. Pompon D, Louerat B, Bronine A, Urban P 1996 Yeast expression of animal and plant P450s in optimized redox environments. Methods Enzymol 272:51–64
72. Urban P, Truan G, Gautier JC, Pompon D 1993 Xenobiotic metabolism in humanized yeast: engineered yeast cells producing human NADPH-cytochrome P-450 reductase, cytochrome b5, epoxide hydrolase and P-450s. Biochem Soc Trans 21:1028–1034
73. Harada N 1988 Novel properties of human placental aromatase as cytochrome P-450: purification and characterization of a unique form of aromatase. J Biochem (Tokyo) 103:106–133
74. Yano JK, Wester MR, Schoch GA, Griffin KJ, Stout CD, Johnson EF 2004 The structure of human microsomal cytochrome P450 3A4 determined by x-ray crystallography to 2.05-A resolution. J Biol Chem 279:38091–38094
75. Scott EE, White MA, He YA, Johnson EF, Stout CD, Halpert JR 2004 Structure of mammalian cytochrome P450 2B4 complexed with 4-(4-chlorophenyl)imidazole at 1.9-A resolution: insight into the range of P450 conformations and the coordination of redox partner binding. J Biol Chem 279:27294–27301
76. Chenna R, Sugawara H, Koike T, Lopez R, Gibson TJ, Higgins DG, Thompson JD 2003 Multiple sequence alignment with the Clustal series of programs. Nucleic Acids Res 31:3497–3500
77. Sali A, Blundell TL 1993 Comparative protein modelling by satisfaction of spatial restraints. J Mol Biol 234: 779–815
78. Hooft RW, Vriend G, Sander C, Abola EE 1996 Errors in protein structures. Nature 381:272
79. Eisenberg D, Luthy R, Bowie JU 1997 VERIFY3D: assessment of protein models with three-dimensional profiles. Methods Enzymol 277:396–404
80. Morris AL, MacArthur MW, Hutchinson EG, Thornton JM 1992 Stereochemical quality of protein structure coordinates. Proteins 12:345–364
81. Ramachandran GN, Ramakrishnan C, Sasisekharan V 1963 Stereochemistry of polypeptide chain configurations. J Mol Biol 7:95–99
82. Hooft RW, Sander C, Vriend G 1997 Objectively judging the quality of a protein structure from a Ramachandran plot. Comput Appl Biosci 13:425–430
83. Holm L, Park J 2000 DaliLite workbench for protein structure comparison. Bioinformatics 16:566–567
84. Guex N, Peitsch MC 1997 SWISS-MODEL and the Swiss-PdbViewer: an environment for comparative protein modeling. Electrophoresis 18:2714–2723
85. Vriend G 1990 WHAT IF: a molecular modeling and drug design program. J Mol Graph 8:52- 56:29
86. Krieger E, Darden T, Nabuurs SB, Finkelstein A, Vriend G 2004 Making optimal use of empirical energy functions: force-field parameterization in crystal space. Proteins 57:678–683
87. Liu H, Elstner M, Kaxiras E, Frauenheim T, Hermans J, Yang W 2001 Quantum mechanics simulation of protein dynamics on long timescale. Proteins 44:484–489
88. Rowland P, Blaney FE, Smyth MG, Jones JJ, Leydon VR, Oxbrow AK, Lewis CJ, Tennant MG, Modi S, Eggleston DS, Chenery RJ, Bridges AM 2006 Crystal structure of human cytochrome P450 2D6. J Biol Chem 281: 7614–7622
89. Schneidman-Duhovny D, Inbar Y, Polak V, Shatsky M, Halperin I, Benyamini H, Barzilai A, Dror O, Haspel N, Nussinov R, Wolfson HJ 2003 Taking geometry to its edge: fast unbound rigid (and hinge-bent) docking. Proteins 52:107–112
90. Mustard D, Ritchie DW 2005 Docking essential dynamics eigenstructures. Proteins 60:269–274

Molecular Endocrinology **is published monthly by The Endocrine Society (http://www.endo-society.org), the foremost professional society serving the endocrine community.**